AGU PUBLICATIONS

Water Resources Research

RESEARCH ARTICLE
10.1002/2017WR020975

Key Points:
- Tidal and offshore storm pulse signal propagation analysis used to characterize coastal aquifer structure
- First time analytical solution for offshore storm-induced water table fluctuations compared to field data for a multilayer coastal aquifer
- Model used to test aquifer characterization and evaluate factors affecting tidal propagation in leaky confined-unconfined aquifers

Supporting Information:
- Supporting Information S1

Correspondence to:
C. E. Robinson,
crobinson@eng.uwo.ca

Citation:
Trglavcnik, V., Morrow, D., Weber, K. P., Li, L., & Robinson, C. E. (2018). Analysis of tide and offshore storm-induced water table fluctuations for structural characterization of a coastal island aquifer. *Water Resources Research*, *54*, 2749–2767. https://doi.org/10.1002/2017WR020975

Received 21 APR 2017
Accepted 8 FEB 2018
Accepted article online 16 FEB 2018
Published online 13 APR 2018

Analysis of Tide and Offshore Storm-Induced Water Table Fluctuations for Structural Characterization of a Coastal Island Aquifer

Victoria Trglavcnik[1], Dean Morrow[2], Kela P. Weber[2], Ling Li[3,4], and Clare E. Robinson[1]

[1]Department of Civil and Environmental Engineering, Western University, London, ON, Canada, [2]Environmental Sciences Group, Department of Chemistry and Chemical Engineering, Royal Military College of Canada, Kingston, ON, Canada, [3]School of Civil Engineering, University of Queensland, Lucia, QLD, Australia, [4]State Key Laboratory of Hydrology-Water Resources and Hydraulic Engineering, Hohai University, Nanjing, China

Abstract Analysis of water table fluctuations can provide important insight into the hydraulic properties and structure of a coastal aquifer system including the connectivity between the aquifer and ocean. This study presents an improved approach for characterizing a permeable heterogeneous coastal aquifer system through analysis of the propagation of the tidal signal, as well as offshore storm pulse signals through a coastal aquifer. Offshore storms produce high wave activity, but are not necessarily linked to significant onshore precipitation. In this study, we focused on offshore storm events during which no onshore precipitation occurred. Extensive groundwater level data collected on a sand barrier island (Sable Island, NS, Canada) show nonuniform discontinuous propagation of the tide and offshore storm pulse signals through the aquifer with isolated inland areas showing enhanced response to both oceanic forcing signals. Propagation analysis suggests that isolated inland water table fluctuations may be caused by localized leakage from a confined aquifer that is connected to the ocean offshore but within the wave setup zone. Two-dimensional groundwater flow simulations were conducted to test the leaky confined-unconfined aquifer conceptualization and to identify the effect of key parameters on tidal signal propagation in leaky confined-unconfined coastal aquifers. This study illustrates that analysis of offshore storm signal propagation, in addition to tidal signal propagation, provides a valuable and low resource approach for large-scale characterization of permeable heterogeneous coastal aquifers. Such an approach is needed for the effective management of coastal environments where water resources are threatened by human activities and the changing climate.

1. Introduction

Coastal groundwater levels fluctuate in response to oceanic forcing including tides (semidiurnal, diurnal, spring-neap), individual high-frequency waves, and variable wave conditions including periods of high wave activity driven by offshore storms (e.g., Cartwright & Gibbes, 2011; Erskine, 1991; Ferris, 1951; Jacob, 1950; Jiao & Tang, 1999; Li et al., 2004; Nielsen, 1990; Raubenheimer et al., 1999; Turner et al., 1997; Van Der Kamp, 1972). These fluctuations impact flows and chemical transport in coastal aquifers, as well as groundwater discharge rates (i.e., submarine groundwater discharge) and associated chemical fluxes to the ocean (e.g., Geng et al., 2014; Li et al., 1999; Moore, 2010; Robinson et al., 2007). The propagation of oceanic forcing signals through a coastal aquifer depends on the nature of the forcing signal (i.e., amplitude and period), connectivity between the aquifer and ocean, and the structure and hydraulic properties of the aquifer (i.e., hydraulic diffusivity).

Propagation of tidal signals through coastal aquifers has been extensively studied (e.g., Carr & Van Der Kamp, 1969; Ferris, 1951; Guo et al., 2010; Hsieh et al., 2015; Jacob, 1950; Kim et al., 2005; Nielsen, 1990; Shih et al., 2008; Turner et al., 1997). As a tidal signal propagates landward through an aquifer, the signal becomes increasingly damped (reduced amplitude) and delayed (phase shift). The rates of amplitude damping and phase shift versus inland distance depend on the tidal signal period, aquifer properties (i.e., storativity S or specific yield S_y, hydraulic conductivity K, aquifer depth d) and structural configuration (i.e., single/multilayered aquifer system). As the hydraulic diffusivity (D; ratio of aquifer transmissivity T to storativity S) is typically larger in confined aquifers relative to unconfined aquifers, the tidal signal often propagates

much further inland in confined aquifers with less amplitude damping and phase shift (Jha et al., 2008; Jiao & Tang, 1999; Li et al., 2002; Raubenheimer et al., 1999).

Numerous analytical solutions of tide-induced water table fluctuations exist for homogeneous, single layer aquifer systems (e.g., Jacob, 1950; Nielsen, 1990; Song et al., 2007). Solutions for permeable multilayer coastal aquifer systems have also been developed and include solutions for submarine confined aquifers (e.g., Guo et al., 2007; Li & Chen, 1991; Van Der Kamp & Gale, 1983), and submarine leaky confined-unconfined aquifer systems (e.g., Asadi-Aghbolaghi et al., 2014; Chuang et al., 2010; Chuang & Yeh, 2008; Jeng et al., 2002; Jiao & Tang, 1999; Li & Jiao, 2001; Sun et al., 2008; Xia et al., 2007). Jiao and Tang (1999) developed an analytical solution for water table fluctuations in a layered system with a permeable unconfined aquifer and confined aquifer separated by a thin aquitard. Assuming a static water table in the unconfined aquifer due to high S_y, they observed rapid propagation through the confined aquifer due to low S. However, the head difference between the permeable aquifer units induced leakage between layers resulting in dampening of head fluctuations in the confined aquifer (Jiao & Tang, 1999). Other studies for multilayer aquifer systems also found that assuming a static water table in the unconfined aquifer results in high damping and slower propagation of pressure fluctuations in the confined aquifer with the extent of dampening varying based on the leakage flux through the aquitard, and ratio of the layered aquifer parameters (S_y/S, unconfined aquifer transmissivity/confined aquifer transmissivity) (Jeng et al., 2002; Li et al., 2001, 2002). Notably, Jeng et al. (2002) and Li et al. (2002) are the only studies that have described the potential for enhanced water table fluctuations in an unconfined aquifer due to leakage of the tidal signal from an underlying confined aquifer.

Generally, most analytical solutions for single and multilayer aquifer systems assume simplified aquifer configurations with few solutions incorporating the effects of a sloping beach face (e.g., Li et al., 2000b; Nielsen, 1990; Teo et al., 2003), vertical flow (Nielsen et al., 1997), and capillarity (e.g., Jeng et al., 2005; Kong et al., 2015; Li et al., 2000a). Further, compared to the numerous analytical studies, there are surprisingly limited field investigations that provide detailed evaluation of tide-induced water table fluctuations in coastal aquifer systems which are typically more complex than those represented by analytical solutions.

Comprehensive understanding of coastal hydrogeology is critical for coastal water resource management including investigations of fresh groundwater availability and coastal aquifer contamination. Aquifer characterization techniques have been developed to estimate aquifer properties (e.g., diffusivity D) based on analysis of water table response to external forces (e.g., barometric fluctuations, tides) (e.g., Carr & Van Der Kamp, 1969; Ferris, 1951). These methods have been widely implemented (e.g., Alcolea et al., 2007; Rotzoll et al., 2008; Slooten et al., 2010; Trefry & Bekele, 2004; Wang et al., 2013) as they are often less-resource intensive relative to other investigative methods (e.g., boring, pumping tests) and can provide information over large length scales. Independent estimates of D can be derived from calculating the rates of tidal attenuation ($D_{amp,}$ amplitude-resolved D) and phase lags ($D_{pha;}$ phase-resolved D) as the signal propagates inland. Considering one-dimensional tidal signal propagation through a homogeneous aquifer, D_{amp} and D_{pha} should be equal (Jacob, 1950); however, discrepancies are often observed due to large and small-scale aquifer heterogeneities, capillarity effects, and shallow aquifer depth (Cartwright et al., 2004; Trefry & Bekele, 2004).

In heterogeneous coastal aquifers, tidal signal propagation analysis alone may not provide sufficient information to adequately characterize the coastal hydrogeology. In this study, we demonstrate that characterization of coastal aquifer structure be improved by also analyzing the propagation of offshore storm pulse signals through a coastal aquifer. Offshore storms generate intensified wave activity at the shoreline but are not necessarily associated with onshore precipitation. Waves lead to an onshore setup of the mean water level within the surf zone due to momentum transfer associated with breaking waves (Longuet-Higgins, 1983). Wave setup elevates the mean water level at the mean shoreline location (termed shoreline setup) to the order of $0.4H_{0rms}$ (root-mean-square deep water wave height) (Hanslow & Nielsen, 1993). Changes in the shoreline setup in response to high wave activity caused by to offshore storms can occur for multiple days and be represented by a pulse signal (herein called a storm pulse) (Li et al., 2004). Similar to tidal fluctuations, this pulse results in water table fluctuations that are increasingly damped and delayed as the storm signal propagates inland (Li et al., 2004). As a storm pulse typically has a longer fluctuation period compared to tidal fluctuations, the pulse signal may propagate farther into an aquifer, and therefore, may provide information over greater distances inland. This was illustrated by Li et al. (2004) who presented an

analytical solution for a homogeneous, isotropic uniform-depth aquifer exposed to a storm pulse signal at a "vertical" beach boundary. Cartwright and Gibbes (2011) compared this analytical solution to field observations in a sandy unconfined aquifer and showed reasonable comparison between the solution and measured propagation of the pulse signal. This analytical solution however has not been applied to field observations in a more heterogeneous coastal aquifer system. To the authors' knowledge, Rotzoll and El-Kadi (2008) is the only study that has attempted to estimate coastal aquifer properties based on analysis of the propagation of wave setup through an aquifer. However, in their analysis they assumed wave setup variations can be represented as a continuous sinusoidal signal rather than discrete pulse signals which better represent offshore storm events.

The objective of this study was to take advantage of key differences between tidal and offshore storm pulse signals by analyzing the propagation of both signals to provide added insight into the structure of a permeable coastal aquifer system. Analysis of both tidal and offshore storm pulse signals has not been done previously, with offshore storm pulse propagation in aquifers having received little attention. Further, there are currently limited studies that have implemented aquifer characterization methods based on analysis of tide-induced water table fluctuations observed in heterogeneous coastal aquifer settings. While a large number of analytical solutions for tidal propagation through single and multilayer aquifer systems exist, they are rarely tested against field data, and field studies typically only analyze propagation of monochromatic tidal signals in sandy unconfined aquifer settings. This study also aims to advance understanding of the propagation of offshore storm pulse forcing through coastal aquifers; this addresses the increasing need to understand the response of coastal groundwater dynamics to offshore storms given predicted climate change effects including the increasing intensity and frequency of storm events (e.g., Danard et al., 2003; Wu et al., 2002). In this paper, data collected from a groundwater monitoring network installed on a sandy barrier island (Sable Island, NS, Canada) are first analyzed to evaluate the propagation of the tidal and offshore storm pulse signals, respectively, and subsequently to infer the structure of the aquifer system. With the results from the dual signal analysis indicating the presence of a leaky confined-unconfined aquifer system at the study site, a two-dimensional numerical groundwater model is then used to test this aquifer conceptualization and to provide insight into key factors controlling tidal signal propagation in this multilayer system. With most coastlines exposed to both tides and waves, the relatively low resource intensive analysis method adopted may be used to improve large-scale characterization of heterogeneous coastal aquifers.

2. Field Description and Methodology

2.1. Field Site

Sable Island is a remote sand barrier island located in the Atlantic Ocean 175 km southeast of mainland Canada (Figure 1a). Sable Island is approximately 42 km long and 1.3 km across at its widest point which results in a groundwater system that is highly influenced by oceanic fluctuations. Sable Island formed from glacial outwash sediments of the Scotian Shelf over the past several thousand years due to sea level rise and local ocean currents (Hennigar, 1976). The island morphology is highly dynamic with historical aerial photos indicating an overall easterly movement of the island. This study focuses on the Main Station and adjacent shoreline areas where the minimal development on the island is located (Figure 1). The Main Station area is characterized by two well-developed sand dune ridges that run parallel to the north and south beaches with low lying gentle undulating topography between these ridges.

The limited drilling records available (all of which are located outside the Main Station area) indicate that Sable Island is underlain by approximately 300 m of Quaternary unconsolidated sands, 900 m of Tertiary sediments and 3,400 m of Cretaceous sediments (Hennigar, 1976). No bedrock outcropping or clay deposits have been reported. The surficial geology is fine poorly graded homogeneous sand (d_{10} = 0.2 mm, coefficient of uniformity [C_u] = 1.5) which results in high aquifer recharge with minimal surface overland flow. Small seasonal and perennial surface water ponds form in some low relief areas with most surface water features being shallow (up to 2–3 m in depth) and of variable quality (brackish and freshwater). Ponds are often lined with low-permeability organic materials (e.g., peat, mud), with large perennial ponds underlain by thick layers of this material (Hennigar, 1976). Horizons of organic material have been observed at various depths below ground surface (up to 18 m deep) and along erosional faces of sand dunes—these may be

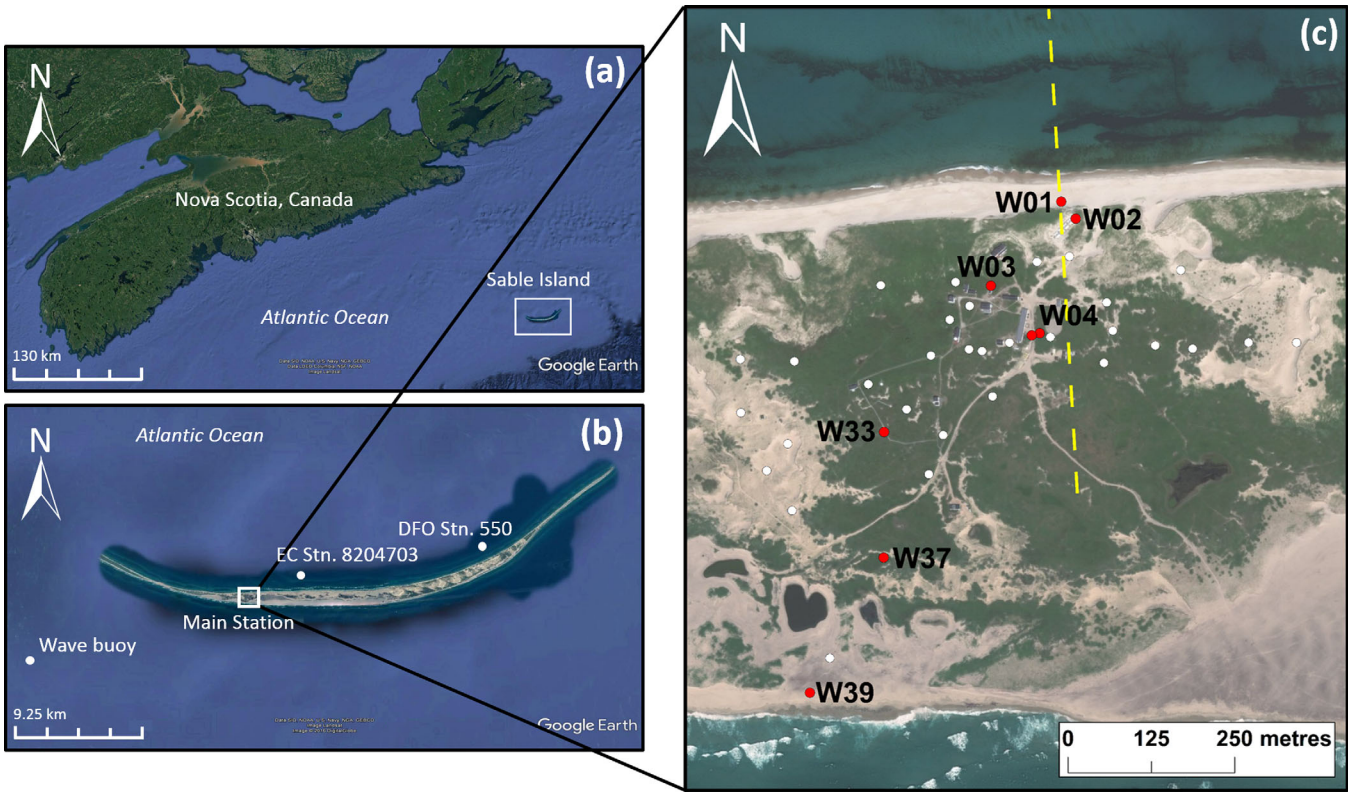

Figure 1. Maps showing (a) location of Sable Island in the Atlantic Ocean relative to Nova Scotia, Canada; (b) locations of the Main Station area, offshore wave buoy, Environment Canada (EC) weather station 8204703, and the Canadian Department of Fisheries and Oceans (DFO) tide gauge station 550; and (c) the Main Station area with locations of continuous long-term monitoring wells indicated by white dots and select wells labeled with their respective I.D.s by red dots. The yellow dash line in Figure 1c indicates the cross-shore transect simulated in the numerical model. Imagery provided by Google Earth in Figures 1a and 1b and Esri Basemaps in Figure 1c.

associated with relic surface water features that have been buried by sand over time as the island morphology shifts (Hennigar, 1976).

Typical for sand barrier islands, the groundwater system is highly dynamic with the water table fluctuating in response to tides and offshore storms. Sable Island is exposed to semidiurnal dominated tides with the tidal range varying between 0.3 and 1.7 m (average = 1.1 m) (Fisheries and Oceans Canada, tides.gc.ca). Local topography, surface water features, and precipitation also impact the water table fluctuations across the island. The hydraulic conductivity (K) of the surficial aquifer was estimated by Hennigar (1976) to be between 1.54 and 95 m/d using various methods (e.g., field pumping and infiltration method). Pumping tests also conducted by Hennigar (1976) at two wells outside of the Main Station area estimated the average transmissivity (T) and S_y to be 462 m^2/d and 0.36, respectively.

2.2. Data Collection

Groundwater level data were obtained from a network of 95 monitoring wells around the Main Station. Groundwater wells were installed along transects that dissect the Main Station from north-to-south (shoreline to shoreline) and east-to-west, with additional wells installed in the central Main Station area (Figure 1b). All groundwater wells were installed in the shallow aquifer up to approximately 1 m below the mean water table. Continuous groundwater level data were collected at 26 wells located across the study area from August 2014 to August 2015. For this, self-logging transducers (CTD-Diver and Mini-Diver, Schlumberger Water Services; Level Troll 700, In-Situ Inc.) were used to measure and record the water pressure and specific conductivity at 20 min intervals. Conductivity data are not presented as data indicated the groundwater in all monitoring wells was fresh or with low salinity (<5 ppt). This is likely due to the shallow installation of the wells and is consistent with geophysical electrical sounding surveys conducted by Hennigar

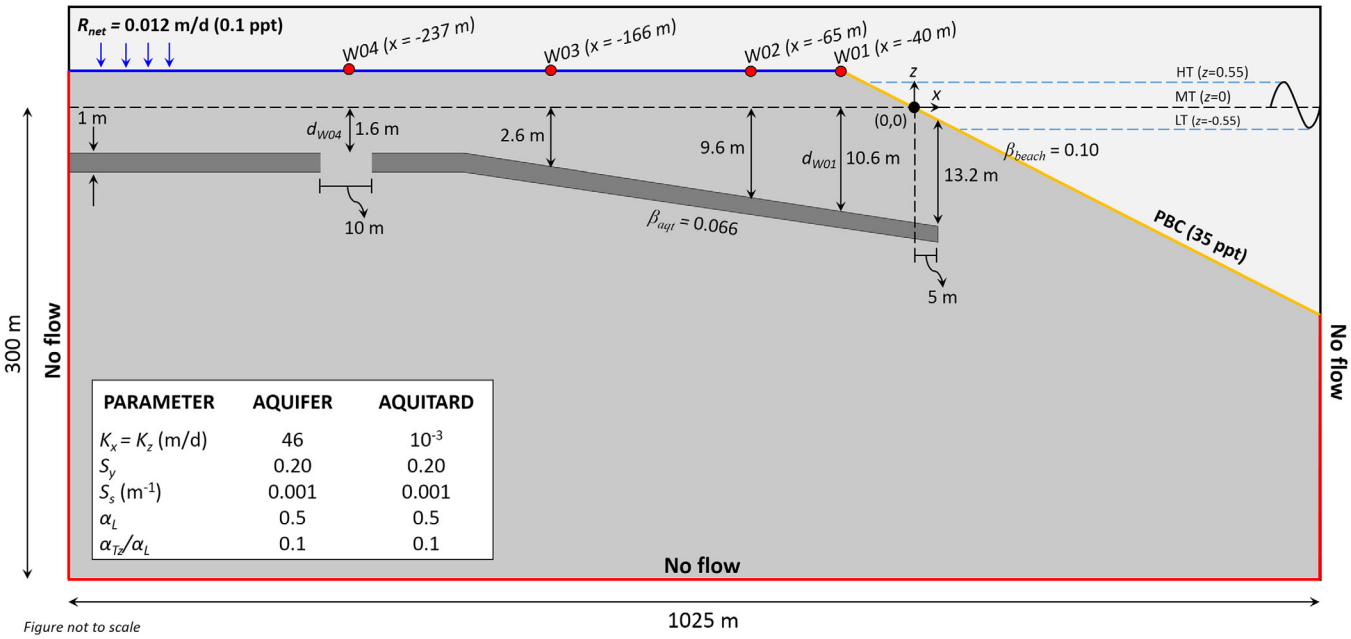

Figure 2. Model domain, boundary conditions and parameters used to simulate a leaky confined-unconfined aquifer system with a discontinuous aquitard layer. This configuration provided the best match between the simulated tidal amplitude attenuation factors (α_t) and calculated α_t from measured data. The aquitard extends 5 m offshore of the estimated mean shoreline position, i.e., the coordinate origin (0,0) at the mean tide level (MT). A tidal boundary condition is applied along the aquifer-ocean interface with the PBC package (Post, 2011) and with $\alpha_{tide} = 0.55$ m and $\omega = 12.14$ rad/d (for semi-diurnal lunar tidal constituent, M2).

(1976) which estimated that the depth of the saltwater wedge (0.5 isochlor) to reach ~36 m across the Main Station area (see supporting information Figure S2). Manual groundwater level measurements and transducer maintenance were performed during four field site visits over the 12 month monitoring period. Self-logging transducers were also installed temporarily (~25 h) in 13 select groundwater wells during these field visits to better quantify the propagation of the tidal signal. Groundwater pressure head data (with barometric pressure fluctuations removed) were converted to groundwater levels referenced to sea level using digital global position satellite (DGPS) surveys, and projected to the North American Datum 1983 (NAD83). The accuracy of converted groundwater levels is estimated to be 0.005 m based on the accuracy of the pressure transducers and DGPS receiver (ESG, 2015). Groundwater level time series were analyzed together with local tide data (Fisheries and Oceans Canada; www.tides.gc.ca), wave data from a buoy located approximately 16 km south of the island (Figure 1b) and precipitation data. Wave data were only available from 9 September to 16 November 2014, and 20 June to 31 August 2015. The tide and wave data are assumed to represent forcing conditions for both the north and south shorelines. Meteorological data (precipitation, wind speed) were obtained from weather stations on Sable Island (Figure 1b) (Environment Canada's National Climate Archives, climate.weather.gc.ca).

2.3. Analysis of Tidal Signal Propagation

Spectral analysis was first applied to groundwater level and tidal level time series to identify the dominant frequencies and tidal constituents in the data. This was done using the discrete Fast Fourier Transform method. Least squares fitting of the groundwater level and tidal level time series to the dominant tidal mode detected (i.e., the Principal Lunar semidiurnal M2 tidal constituent, where one sinusoidal tidal cycle occurs over a period of 12.421 h, frequency $\omega = 12.14$ rad/d) was then conducted to resolve the amplitude and phase of the tide-induced water table fluctuations (e.g., Merritt, 2004; Rotzoll & El-Kadi, 2008). Subsets of the continuous groundwater level data were selected for analysis at all monitoring wells over periods when the groundwater levels did not exhibit strong rising or falling trends associated with recharge, drainage flows and/or evapotranspiration. Remaining, minor trends were removed by linearly detrending data before determining the amplitude and phase of the dominant tidal mode by least squares fitting of data to the harmonic function:

$$h(t) = h_0 + \alpha_i \cos(\omega t + \phi_i) \quad (1)$$

where h is the groundwater level or tidal level fluctuating about h_0 (mean h), α_i is the amplitude of the groundwater level or tidal level fluctuation (α_{GWL} and α_{tide}, respectively), ω is frequency of the tidal component (12.14 rad/d for M2), t is time, and ϕ_i is the phase lag of the groundwater level or tidal level fluctuation in radians (ϕ_{GWL} and ϕ_{tide}, respectively). The tidal efficiency factor (α_t), which describes the attenuation of the tidal signal, and the phase lag $\Delta\phi_t$ (e.g., Erskine, 1991; Merritt, 2004), were calculated at each well location by:

$$\alpha_t = \frac{\alpha_{GWL}}{\alpha_{tide}} \quad (2a)$$

$$\Delta\phi_t = \phi_{GWL} - \phi_{tide} \quad (2b)$$

Where possible, α_t and $\Delta\phi_t$ at a well location were calculated using multiple data subsets to test for stationarity, and mean α_t and $\Delta\phi_t$ were adopted for further analyses.

Calculation of α_t and $\Delta\phi_t$ identified four distinct spatial areas of high ocean-aquifer connectivity: (1) north-shore area, (2) south-shore area, (3) inland area around well W04 (herein called Area 1), and (4) inland area around well W33 (herein called Area 2). Water table fluctuations in these areas were subsequently analyzed individually. Data from wells installed near the north-shore (W01, W02) were used to evaluate tidal signal propagation through the unconfined aquifer; however, data collected near the south-shore (W39) were not analyzed further due to limited spatial data resolution in this area. Data from Areas 1 and 2 were used to test the hypothesis that the rapid propagation of the tidal signal to these inland areas may be caused by upward leakage from a confined aquifer connected to the ocean.

Water table wave numbers k_r and k_i, which are the rates of tidal signal amplitude attenuation and phase lag, respectively, were calculated for the north-shore area, Area 1 and Area 2 by linear regression of $ln(\alpha_t)$ versus x, and $\Delta\phi_t$ versus x, where x is the distance to the shoreline for the north-shore area and to the suspected leakage locations for Areas 1 and 2. According to the linear groundwater wave theory (Ferris, 1951; Jacob, 1950):

$$k_r = k_i = \sqrt{\frac{S_y \omega}{2Kd}} \quad (3)$$

k_r and k_i were then used to estimate the aquifer diffusivity (D) (e.g., Rotzoll et al., 2008):

$$D_{amp} = \frac{\omega}{2k_r^2} \quad (4a)$$

$$D_{pha} = \frac{x^2\omega}{2k_i^2} \quad (4b)$$

Although equation (3) suggests that wave numbers k_r and k_i are equal, field studies often observe $k_r > k_i$ indicating that the tidal signal travels through the aquifer faster (is less lagged) than predicted by the observed tidal damping (Cartwright, 2004). This propagation bias can be quantified by a slope factor (SF):

$$SF = \sqrt{\frac{D_{amp}}{D_{pha}}} \quad (5)$$

2.4. Analysis of Storm Pulse Signal Propagation

Data collected during two offshore storm events (15–21 September 2015 and 1–8 October 2015) were used to quantify the response of the groundwater levels to a storm pulse. These two events were chosen because there was no onshore precipitation around the same time, and therefore the observed nontidal groundwater level changes could be attributed solely to storm pulse forcing. A low-pass Hamming filter was first applied to the groundwater level time series to remove high-frequency fluctuations including those associated with tides (e.g., Crosbie et al., 2005). Offshore significant wave height (H_s, m) and peak period (T_p, sec) data were used to calculate shoreline setup, η_s, using the relationship (Hanslow & Nielsen, 1993):

$$\eta_s = 0.048\sqrt{H_{0rms}L_0} \tag{6}$$

where H_{0rms} is the root-mean-squared deep water wave height (calculated as $H_{0rms} = H_s/\sqrt{2}$) and L_0 is the deep water wavelength (calculated as $L_0 = gT_p^2/2\pi$). Time series of shoreline elevation, z_{SL}, was then calculated by:

$$z_{SL} = z_{tide} + \eta_s \tag{7}$$

where z_{tide} is the tidal level (in meters above sea level, masl). Shoreline elevation data were also filtered using a low-pass Hamming filter before comparing with the filtered groundwater level data.

The amplitude and time lag of the storm pulse signal at individual wells was determined by least squares fitting the filtered groundwater levels and shoreline elevation (z_{SL}) during the two storm events to a pulse function of the form:

$$h(t) = h_0 + A\exp\left[-B\left(t - t_p\right)^2\right] \tag{8}$$

where h is water level (groundwater or shoreline elevation) fluctuating about h_0 (mean h), A is the amplitude of the pulse, B is a time factor (B^{-2} reflects the duration of the storm event or groundwater level response), and t_p is the time when peak h occurs (Li et al., 2004). Following Cartwright and Gibbes (2011), only the rising limb of groundwater level and shoreline elevation data were considered in the fitting analysis because temporal asymmetry in groundwater level pulses (due to rapid aquifer filling compared with slow drainage) are not well described by the pulse function. The attenuation (α_w) and time lag ($\Delta\phi_w$) of the storm pulse through the aquifer were quantified by:

$$\alpha_w = \frac{A_{GWL}}{A_{SL}} \tag{9a}$$

$$\Delta\phi_w = t_{p,GWL} - t_{p,SL} \tag{9b}$$

where A_{GWL} and A_{SL} are the amplitude of groundwater level and shoreline elevation pulses, respectively, and $t_{p,GWL}$ and $t_{p,SL}$ are the time of the peak groundwater level and shoreline elevation, respectively.

To evaluate the homogeneity of the coastal aquifer, field observations were compared to an analytical solution developed by Li et al. (2004) for a homogeneous unconfined aquifer exposed to a storm pulse signal (with beach slope effects neglected):

$$h(x,t) = -2AB\int_{-\infty}^{t}\left(\tau - t_p\right)\exp\left[-B\left(\tau - t_p\right)^2 erfc\left[\frac{x}{2\sqrt{D(t-\tau)}}\right]d\tau\right. \tag{10}$$

where x is distance from the mean shoreline position. Details on the analytical solution including boundary and initial conditions are provided in Li et al. (2004). A nondimensionalized form of equation (10) was used to compare propagation of the storm pulse for different duration offshore storms (e.g., different B) (Li et al., 2004). Following Li et al. (2004) nondimensional time lag ($\Delta\phi_w^*$) and nondimensional distance from the shoreline (x^*) were calculated as:

$$\Delta\phi_w^* = \Delta\phi_w\sqrt{B} \tag{11a}$$

$$x^* = \frac{x}{2\sqrt{D/B^{1/2}}} \tag{11b}$$

using storm pulse parameter B that was determined by fitting the z_{SL} data to equation (8).

2.5. Numerical Groundwater Flow Modeling

A two-dimensional variable-density groundwater flow model was developed to simulate tidal signal propagation in the aquifer system with the aim to test the validity of the aquifer hydrogeological characterization (i.e., leaky confined-unconfined aquifer) inferred from the analysis of tidal and storm pulse signal propagation. The objective of the model was not to simulate the three-dimensional groundwater flow and replicate measured groundwater heads across the study site subjected to the influence of multiple forcing, but rather, to demonstrate the plausibility of the multilayer hydrogeological characterization of the aquifer

inferred from the data analysis. Simulations based on the model investigated tidal signal propagation through the leaky confined-unconfined aquifer configuration under a range of conditions. The interactions among different forcing factors affect little the tidal signal propagation over the time scale examined here. For example, the water table in the upper unconfined aquifer may rise and fall due to recharge. However, this only leads to relatively small changes in the overall aquifer depth over the period considered in the analysis and thus makes negligible difference to the tidal signal propagation characteristics in terms of both amplitude damping and phase shift (Nielsen, 2009). The model was implemented in SEAWAT Version 4 (Langevin et al., 2008). The model domain represents a vertical cross-shore section through a unit width of aquifer (Figure 2), analogous to simulating a transect through the north beach on Sable Island (Figure 1c). A suite of simulations were conducted with varying unconfined and confined aquifer depths, configuration of the aquitard layer (depth, slope [β_{aqt}], width and location of discontinuity, hydraulic conductivity [K_{aqt}]), distributed recharge rate, and aquifer specific yield (S_y) (see supporting information Text S2, for details). For each simulation, the absolute differences between the calculated (field) and simulated α_t were compared for four wells located along the cross-shore transect (W01, W02, W03, and W04; Figure 2). While some well locations are slightly offset from the simulated cross-shore transect (Figure 1c), data from additional wells installed on either side of the simulated cross-shore transect suggest that the observed fluctuations are consistent in the shore-parallel direction (except at the inland Areas 1 and 2). Therefore, comparison of the simulation results with this well data is acceptable. Simulated salt concentrations were also compared to the location of the saltwater wedge inferred from geophysical electrical sounding surveys conducted by Hennigar (1976).

For all models, K in the confined and unconfined aquifers was set to 46 m/d based on infiltration tests by Hennigar (1976). The longitudinal (α_L) and transverse dispersivity (α_T) were set to 0.5 and 0.05 m based on dispersion values estimated by Gelhar et al. (1992). Specific storage (S_s) was set to 0.001 m^{-1} for the aquifer and aquitard units and specific yield (S_y) was varied from 0.2 to 0.36. No-flow boundary conditions were applied along the bottom, landward, and vertical seaward boundaries of the domain (e.g., Figure 2). A tidal boundary condition was implemented along the submerged sloping aquifer-ocean interface (beach face) using the Periodic Boundary Condition (PBC) package (Mulligan et al., 2011; Post, 2011; Röper et al., 2015)

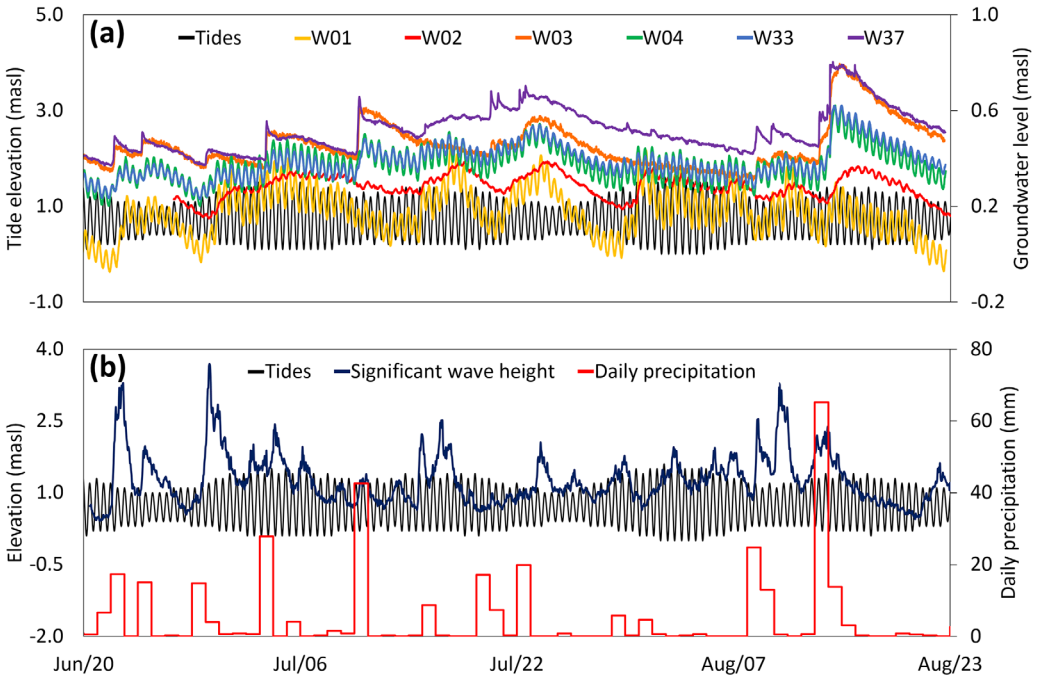

Figure 3. Continuous data of (a) tidal level and groundwater levels, measured in meters above sea level (masl) for select wells; (b) significant wave height (m), tidal level (masl), and daily precipitation (mm) from 20 June to 21 August 2015. This is a subset of the total data recording period which extended from 7 August 2014 to 23 August 2015. Locations of groundwater monitoring wells are shown in Figure 1.

and with a single harmonic tidal signal with α_{tide} = 0.55 m (corresponding to the average tidal amplitude) and ω = 12.14 rad/d (M2 tidal constituent). For influx across the boundary the salt concentration was constant at 35 ppt. For efflux (discharge) across the boundary a no dispersive flux condition was applied (Post, 2011). The slope of the aquifer-ocean interface (β_{beach}) was set to 0.10. Distributed recharge was applied to the top model boundary with the recharge rate varied between 0 and 0.0053 m/d. The recharge rate was estimated to range from 0.0012 to 0.0053 m/d by applying the methods of Crosbie et al. (2005) to groundwater level and precipitation time series. Recharge water had a salt concentration of 0.1 ppt. Additional details on the model setup for the sensitivity simulations are provided in section 3.4 and supporting information Text S2.

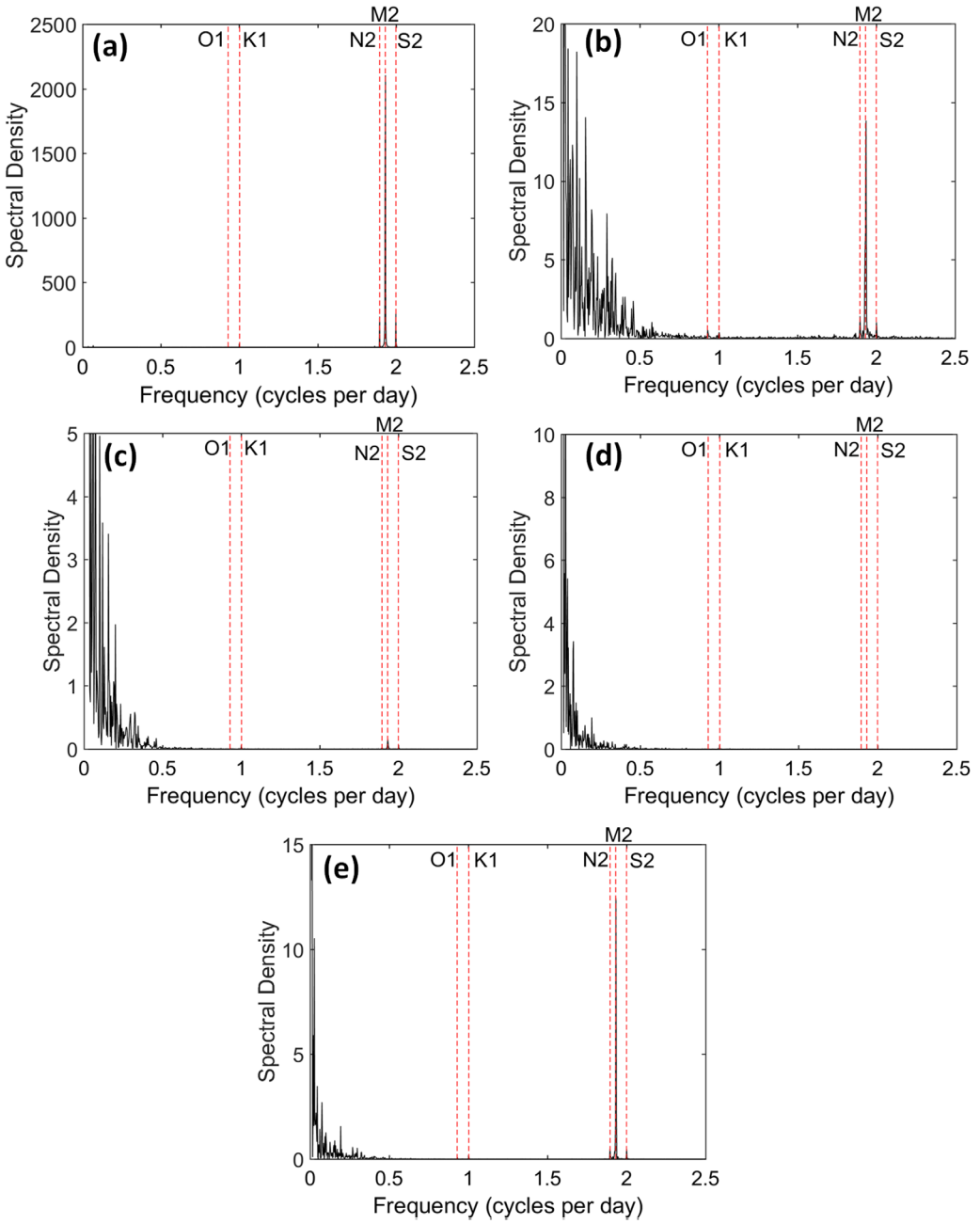

Figure 4. Spectral density plots for (a) tide height data and groundwater monitoring wells data for (b) W01; (c) W02; (d) W03; (e) W04. Known frequencies of tidal constituents (O1, K1, N2, M2, S2) are labeled by red dashed lines.

The model was first run to steady state with no tidal fluctuations. Tidal fluctuations were then simulated for 60 days—this simulation time was sufficient for the aquifer system to reach the quasi-steady state with respect to the water table fluctuations. Grid discretization tests were performed to ensure that the model solution was converged.

3. Results and Discussion

3.1. Response of Groundwater Levels to Key Environmental Forcing

A 2 month subset of groundwater level data measured for selected wells (locations indicated in Figure 1c) are shown in Figure 3 together with time series of tide elevation, significant wave height, and daily precipitation. Contours of mean groundwater levels using data for all continuously monitored wells across the Main Station area are provided in the supporting information Figure S1. As expected the groundwater levels near the shorelines (W01, ~40 m from north shoreline) experience the largest fluctuations in response to the semidiurnal tidal signal and storm events (i.e., periods of high significant wave height) compared to inland groundwater levels. Groundwater level variations at wells further inland (e.g., W03 and W37 located

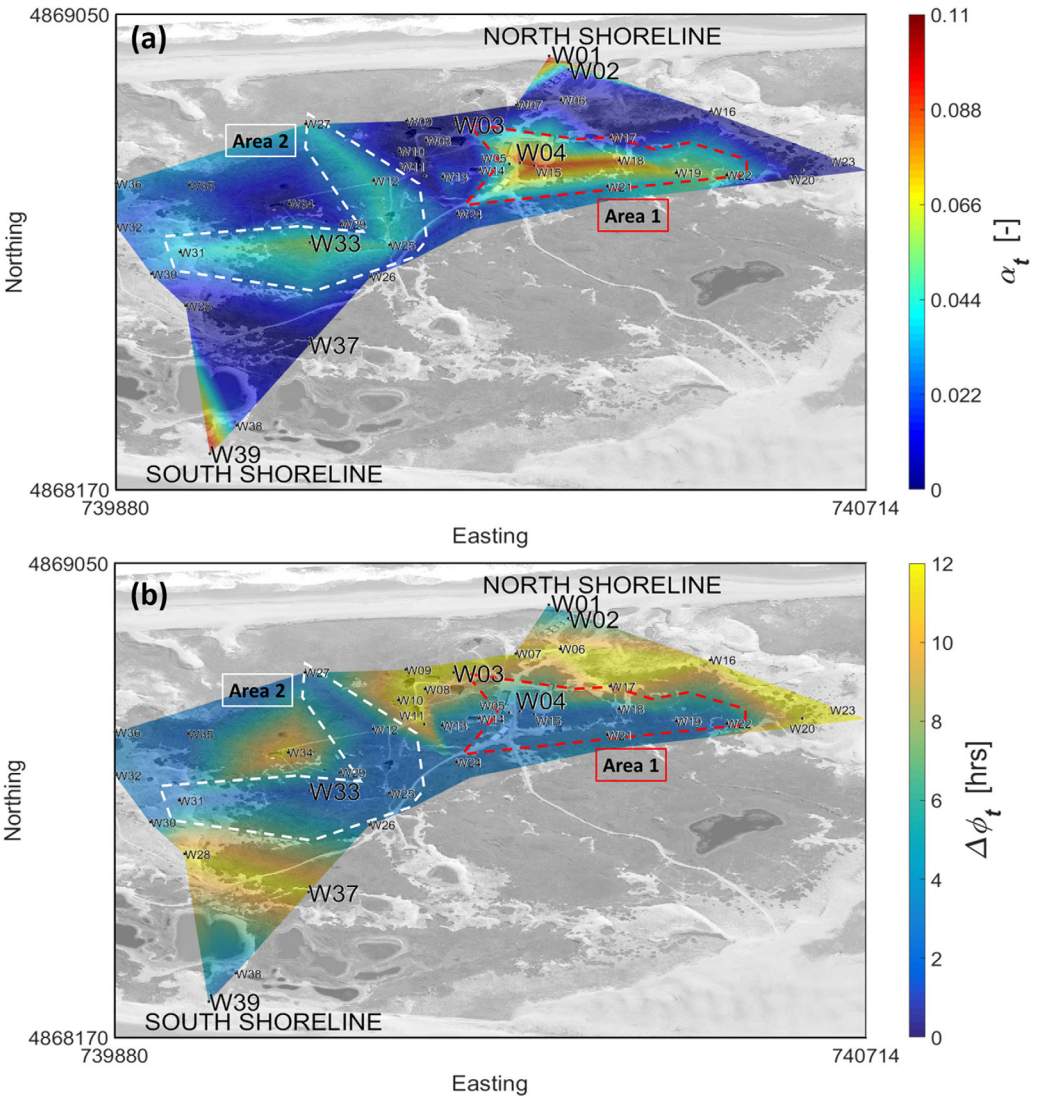

Figure 5. Tidal signal propagation across the Main Station area on Sable Island. Colored contours represent (a) amplitude attenuation ratio (α_t) [–] and (b) phase lag ($\Delta\phi_t$) [h] of groundwater level fluctuation relative to the dominant M2 tidal signal ($\omega = 12.14$ rad/d). Larger α_t and smaller $\Delta\phi_t$ indicate greater and faster groundwater level response to the tidal signal, respectively. Tidal source Area 1 is outlined by a red dash line, and Area 2 is outlined by a white dash line.

~166 and ~270 m from the shoreline, respectively) are mostly attributed to precipitation patterns with limited response to tides and offshore storms. Importantly, strong semidiurnal groundwater level fluctuations are evident at isolated inland locations indicating nonuniform discontinuous propagation of the tidal signal through the coastal aquifer system (e.g., W04 and W33 located ~235 and ~385 m from the shoreline, respectively; Figure 3a).

3.2. Tidal Signal Propagation Analysis

For tidal data, maximum spectra are detected at a frequency of 1.932 cycles per day [cpd], which corresponds to the Principal Lunar semidiurnal M2 tidal constituent (Figure 4a). Smaller spectra are detected at a frequency of 2 cpd corresponding to the Principal Solar S2 tidal constituent, and at 1.896 cpd corresponding to the Larger Lunar Elliptic semidiurnal N2 tidal constituent (Figure 4a). Groundwater level data at W01 also show a distinct peak at the M2 frequency indicating, as expected, high aquifer-ocean connectivity due to the well's close proximity to the shoreline (Figure 4b). The tidal signal is attenuated inland as shown by a decrease in spectral density at the M2 frequency with increasing distance inland (i.e., spectra for W02 and W03, Figures 4c and 4d). However, inconsistent with continuous tidal propagation through an unconfined aquifer, a strong spectral peak corresponding to the M2 frequency is detected at some wells located farther inland (i.e., spectra for W04, Figure 4e). Low-frequency (i.e., 0–0.5 cpd) spectra detected in all groundwater level time series are due to other environmental forcing, such as seasonal precipitation patterns, individual precipitation events, and evapotranspiration.

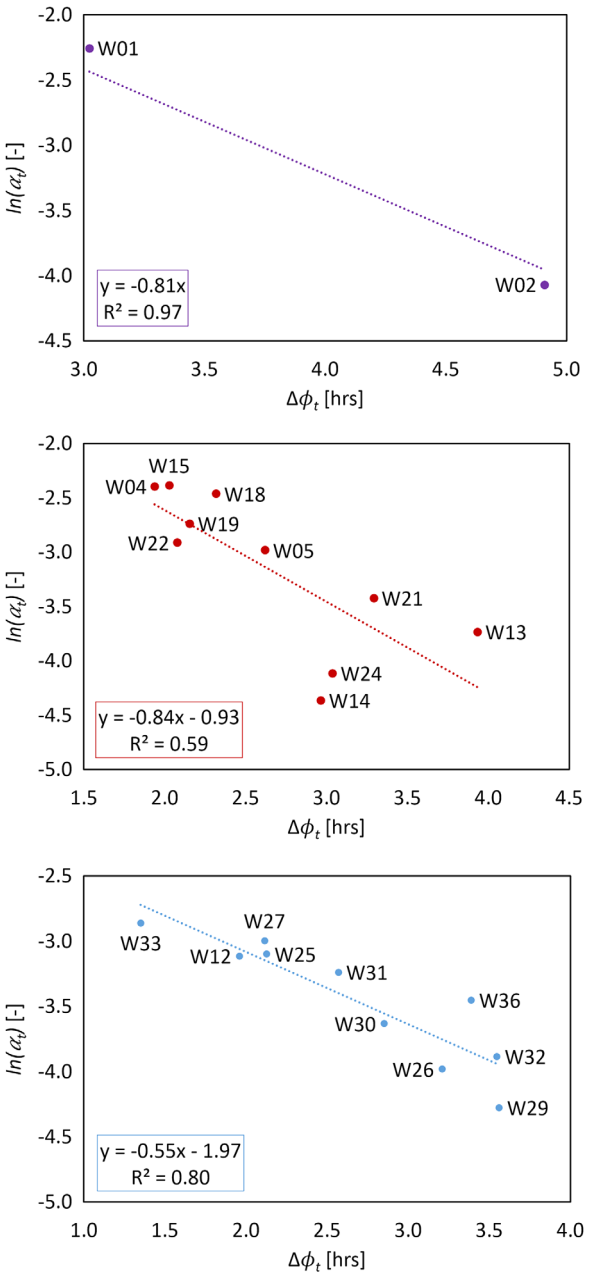

Figure 6. Calculated amplitude attenuation (α_t) [-] versus phase lag $(\Delta\phi_t)$ [h] for groundwater monitoring wells located in tide-influenced areas (a) adjacent to the north beach shoreline, (b) Area 1, and (c) Area 2.

Spatial contour maps of α_t and $\Delta\phi_t$ values show the propagation of the tidal signal (M2 frequency) through the Main Station (Figure 5). Groundwater wells near the north and south shorelines experience the largest tide-induced water table fluctuations and shortest time lags (e.g., $\alpha_t = 0.11$ and $\Delta\phi_t = 4.8$ h at W01). While tide-induced water table fluctuations are damped and delayed with increasing distance inland (e.g., $\alpha_t = 0.017$ and $\Delta\phi_t = 5.9$ h at W02), tide-induced water table fluctuations occur at isolated inland locations as indicated by relatively high α_t and low $\Delta\phi_t$ values (Figure 5, $\alpha_t = 0.091$ and $\Delta\phi_t = 1.9$ h at W04; and $\alpha_t = 0.057$ and $\Delta\phi_t = 1.4$ h at W33). The discontinuous propagation of the tidal signal across the study area suggests that the aquifer system is not a single layer unconfined aquifer system as suggested in prior hydrogeological studies of Sable Island (e.g., Hennigar, 1976). Two distinct isolated inland areas (Areas 1 and 2; Figure 5) can be identified that have large tide-induced water table fluctuations. In these areas, the tide-induced water table fluctuations are of amplitudes similar to that observed near the north-shore (W01), and importantly are less lagged than W01 relative to the driving tidal signal.

In barrier islands, propagation of the tidal signal from opposing shorelines can interfere causing complex tidal signal propagation (e.g., Chang et al., 2010; Huang et al., 2012; Rotzoll et al., 2008; Trefry & Bekele, 2004). However, data indicate that dual signal interference does not occur at our study site as the tidal signal is rapidly damped in the unconfined aquifer with increasing distance from the north and south shorelines (i.e., W06 and W37, Figure 5). While surface water features and complex land topography can also cause nonuniform tidal propagation (Kong et al., 2015), these factors do not explain the isolated nature of the tide-induced water table fluctuations observed in Areas 1 and 2. Rather, data indicate that fluctuations in Areas 1 and 2

Table 1
Aquifer Diffusivity (D) and Slope Factor (SF) Calculated From Amplitude-Resolved (k_r) and Phase-Resolved (k_i) Wave Numbers

Tidal area	k_r	k_i	D_{amp} (m^2/d)	D_{pha} (m^2/d)	SF
North-shore	0.061	0.075	1,660	1,073	1.24
Area 1	0.020	0.016	15,500	24,900	0.79
Area 2	0.018	0.037	18,500	4,360	2.06

may be due to leakage of the tidal pressure signal from an underlying confined aquifer (Jeng et al., 2002). It is possible that the burial of organic layers associated with relic surface water ponds may have led to the formation of a confined-unconfined aquifer system with discontinuities (i.e., gaps or thinning) in the aquitard separating the permeable aquifer units, and causing the observed nonuniform tidal signal propagation. Given the spatial resolution of the monitoring wells it is not possible to determine the spatial extent of the discontinuities in the aquitard. However, the data suggest that the discontinuities result in an inland tidal signal in the form of a line source. This is consistent with leakage that could occur at the edge of a buried relic surface water feature.

Further analysis shows that for all of the tide-influenced areas (i.e., north-shore, Area 1, Area 2) $ln(\alpha_t)$ and $\Delta\phi_t$ are well correlated with the attenuation of the tidal signal increasing with the phase lag (Figure 6). Data from only two wells are shown for the north-shore area (Figure 6a) as the tidal signal was rapidly damped inland of the shoreline, and therefore, wells further landward (i.e., W3 at ~120 m from shoreline) showed negligible fluctuations and could not be included in the analysis. For Areas 1 and 2 (Figures 6b and 6c), deviation from the linear relationship predicted by groundwater wave theory (Ferris, 1951; Jacob, 1950) may be due to nonlinear effects associated with the tidal pressure signal leaking upward from a confined aquifer.

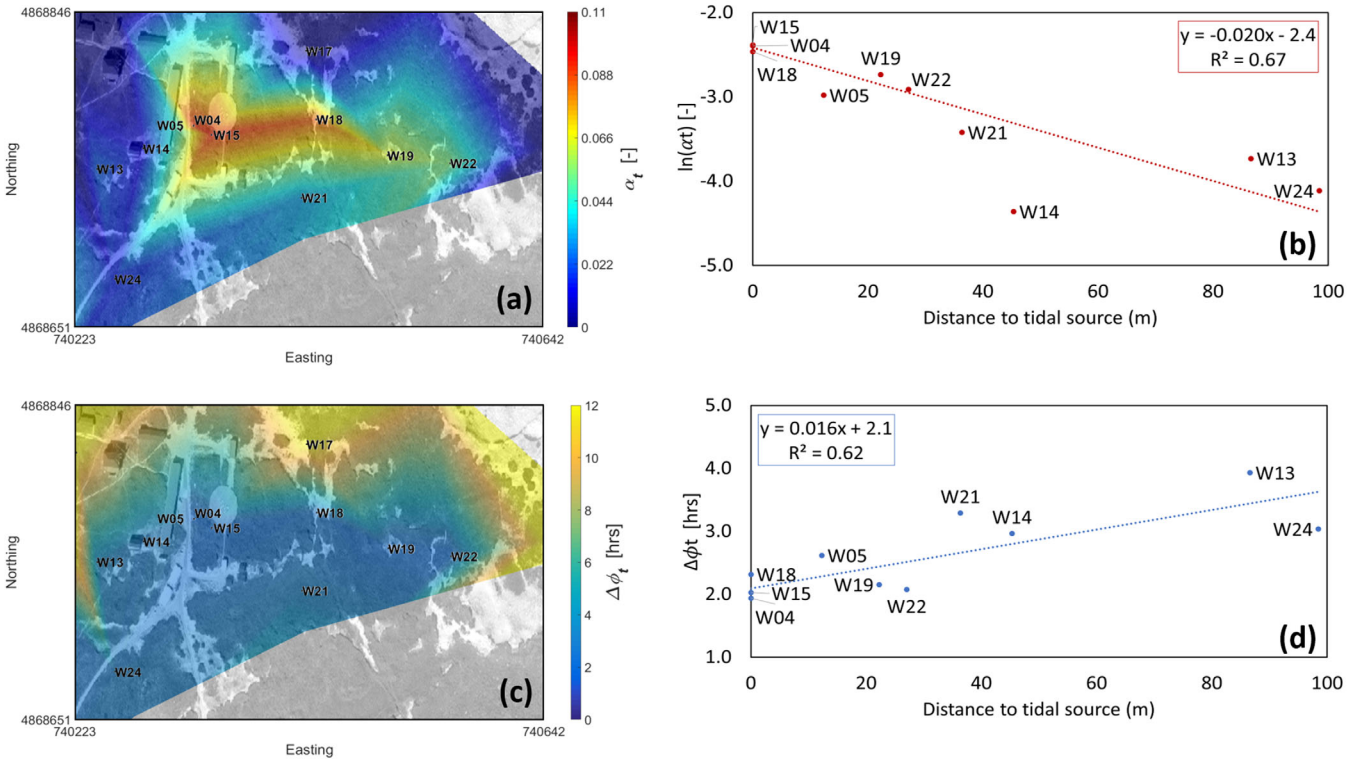

Figure 7. Colored contours of calculated (a) amplitude attenuation (α_t) [–] and (c) phase lag ($\Delta\phi_t$) [h] for Area 1, as an example of an inland tide-influenced area. $ln(\alpha_t)$ and $\Delta\phi_t$ versus distance (x) to hypothesized inland line source are shown in Figures 7b and 7d. Slope of linear regression lines in Figures 7b and 7d estimate wave numbers k_r and k_i, respectively.

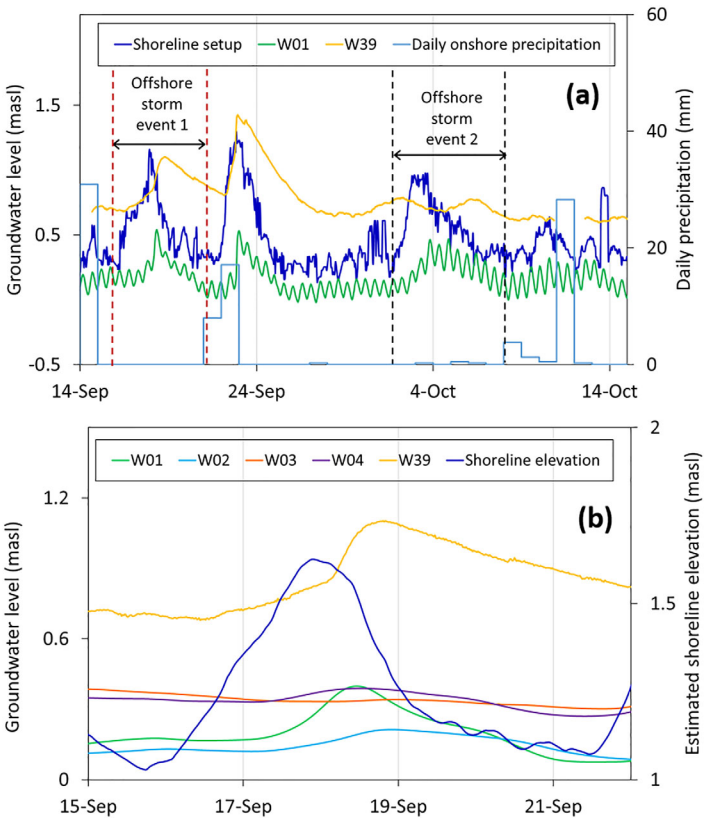

Figure 8. (a) Groundwater levels in meters above sea level (masl), near the north (W01) and south (W39) shorelines, calculated shoreline setup (η_s, m), and daily onshore precipitation (mm) from 14 September to 15 October 2014. Dash lines show durations of offshore storm event 1 (15–21 September) and event 2 (1–8 October) analyzed. (b) Filtered groundwater levels (masl) and calculated shoreline elevation (z_{SL}, masl) for offshore storm event 1.

Calculated values for k_r, k_i, D, and SF are provided in Table 1 for the three tide-influenced areas (north-shore, Areas 1 and 2). Plots of $\ln(\alpha_t)$ and $\Delta\phi_t$ versus distance to the inland tidal line source for Area 1 are shown in Figures 7a and 7b, respectively, to illustrate how the water table wave numbers k_r (rate of amplitude attenuation) and k_i (rate of phase lag) were calculated. The SF values deviate from unity in the three areas. Previous studies have also observed SF values ranging from 0.31 to 3.8 (e.g., Carr & Van Der Kamp, 1969; Cartwright & Gibbes, 2011; Erskine, 1991; Ferris, 1951; Rotzoll et al., 2008; Trefry & Bekele, 2004) with Trefry and Bekele (2004) indicating that macroscale horizontal layering may have caused the propagation bias they observed ($SF = 0.43$, sand and limestone island aquifer). These results further suggest that the aquifer system is not homogeneous. Rapid attenuation of the tidal signal in north-shore area, particularly between W01 and W02, together with the calculated propagation bias ($SF = 1.24$; Table 1) suggests that the unconfined aquifer near the shore may be of nonuniform thickness perhaps due to a sloping aquitard (this is examined in section 3.4).

3.3. Storm Pulse Signal Propagation Analysis

Groundwater level data show pulse-like fluctuations in response to individual offshore storm events and associated shoreline setup (Figure 8). Based on calculated pulse attenuation (α_w) values for the monitoring wells, the storm pulse signal is observed to propagate farther through the unconfined aquifer from the north-shore compared to the tidal signal—this is consistent with the analytical solution of Li et al. (2004). Consistent with the propagation of the tidal signal, storm pulse propagation across the island is nonuniform and discontinuous with the storm pulse fluctuations at W04 (Area 1) less attenuated and less lagged compared to, for example, W03 which is located closer to the shore (Figure 8b). Importantly, the pulse signal travels rapidly to W04 with similar time lag (average $\Delta\phi_w^* = 0.65$) compared to the pulse signal observed at W01 (average $\Delta\phi_w^* = 0.71$) which is located only 40 m from the north shoreline. Although the time lags were similar, fluctuations at W04 are considerably more damped (average $\alpha_w = 0.096$) compared to W01 (average $\alpha_w = 0.42$). This contrasts with the tidal propagation analysis where both α_t and $\Delta\phi_t$ are similar for W04 and W01. Values calculated for other wells located in the inland tide-influenced areas (Areas 1 and 2) show similar trends to W04 (i.e., small α_w, small $\Delta\phi_w^*$). This result suggests that the storm pulse signal may be rapidly propagating inland through a confined aquifer with the pressure signal being transmitted upward to an unconfined aquifer via a leakage features within Areas 1 and 2. Furthermore, the greater attenuation of the storm pulse signal in Areas 1 and 2 compared to W01, despite similar phase lags to W01 for both the tide and storm pulse signals, may be due to the confined aquifer being exposed to a weaker driving storm pulse forcing signal at the seaward boundary. This may occur if the confined aquifer is connected to the ocean seaward of the shoreline, as this would mean the magnitude of the pulse force acting on the confined aquifer would be less than the shoreline setup pulse force acting on the unconfined aquifer due to the wave setup profile (this is discussed in section 3.4).

The analytical solution of Li et al. (2004) (equation (10)) was compared to α_w and $\Delta\phi_w^*$ in nondimensional form based on equations (11a) and (11b) with $D = 1{,}280$ m^2/d (Hennigar, 1976) (Figure 9). While the overall trends for the calculated values and analytical solution are consistent, the match is poor. Calculated α_w values are better predicted by the analytical solution compared to calculated $\Delta\phi_w^*$. While some disagreement between calculated $\Delta\phi_w^*$ and α_w, and the analytical solution may be attributed to nonlinear effects (i.e., sloping beach, finite aquifer depth) (Cartwright & Gibbes, 2011), the disagreement further suggests that the aquifer system is not a single layer unconfined system. The results also suggest further work is required to develop an analytical solution of storm pulse propagation that incorporates nonlinear effects including

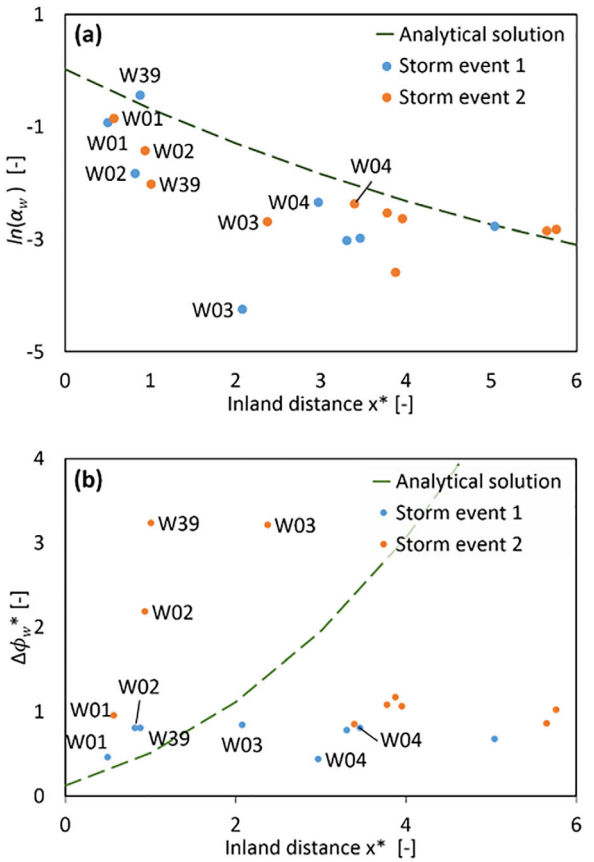

Figure 9. Analysis of storm pulse propagation for two offshore storm events (a) $ln(\alpha_w)$ [–] versus nondimensionalized inland distance (x^*) [–], and (b) $\Delta\phi_w^*$ [–] versus x^*. Calculated values are shown for all monitoring wells with labels only provided for select monitoring wells. Results are compared with the analytical solution of Li et al. (2004) (green dashed line).

heterogeneous aquifer conditions, a sloping beach boundary and moving shoreline position. Compared to the large number of studies focused on tide-induced water table fluctuations, there is limited understanding of storm pulse propagation through coastal aquifers, despite past knowledge that wave-induced storm pulses also drive water table fluctuations in coastal environments (e.g., Cartwright & Gibbes, 2011; Gourlay, 1992; Li & Barry, 2000; Li et al., 2004; Nielsen, 2009).

3.4. Conceptual Model and Numerical Groundwater Flow Simulations

The tide and storm pulse signal propagation analysis indicates that the study area may be characterized as a confined-unconfined aquifer system with isolated discontinuities in an aquitard layer that separates the unconfined and confined units (Figure 10). As the morphology of Sable Island is highly dynamic, it is possible that the burial of low-permeability organic material associated with relic surface water features may have created such an aquitard at depth. The distribution of buried organic material (i.e., discontinuities, and varying depth and thickness) may cause the nonuniform propagation of the tidal and storm pulse signals. Furthermore, comparison of signal attenuation and phase lags for tides (α_t, $\Delta\phi_t$) and storm pulses (α_w, $\Delta\phi_w$) (sections 3.2 and 3.3) suggests that the confined aquifer may be connected to the ocean seaward of the shoreline (i.e., wells in inland Areas 1 and 2 show storm pulse response that is damped compared to wells near the shoreline but with similar time lag). As conceptually illustrated in Figure 10, for a storm pulse, the amplitude of the forcing signal will be greatest if the signal propagates inland from the shoreline (i.e., shoreline setup). If the connection between the aquifer and ocean occurs offshore, as in the case for a submarine confined aquifer, the magnitude of the driving storm pulse forcing, and thus inland storm pulse response, decreases due to the wave setup profile. Based on calculated tide and storm signal propagation ratios, together with the approximate wave setup profile (Nielsen, 2009) and surf zone width (Dean & Dalrymple, 1984) for the storm events analyzed, it is estimated that that the aquitard layer at the study site may extend 5 m offshore from the mean shoreline position (see Text S3 in the supporting information for details of these calculations).

Numerical simulations were conducted to test the conceptualization of a leaky confined-unconfined aquifer system with the aquitard layer extending 5 m seaward of the mean shoreline position. A suite of simulations were conducted with varying structural configurations and aquifer parameters (e.g., unconfined and confined aquifer thickness, configuration of the aquitard and leakage feature, distributed recharge rate). Results for select simulations are provided in Table 2 (see Table S1 in the supporting information for all simulation results). The absolute errors between the simulated and calculated α_t for monitoring wells were lowest using the model setup shown in Figure 2 (case 1, Table 2; herein referred to as the final model). For the final model, a 1 m thick, low-permeability aquitard ($K_{aqt} = 0.001$ m/d) extends across the model domain. The aquitard layer slopes downward near the shoreline ($\beta_{aqt} = 0.066$) such that the thickness of the unconfined aquifer is 10.6 m near the shoreline (i.e., d_{W01} at W01) and 1.6 m further inland (i.e., d_{W04} at W04). A 10 m wide discontinuity in the aquitard is centered below W04. The agreement between the simulated α_t based on the final model configuration, and the calculated (field) α_t for the monitoring wells W01–W04 is shown in Figure 11. For comparison, the simulated α_t for the single layer unconfined aquifer scenario (no aquitard, case 2 in Table 2) are also shown in Figure 11. For this scenario α_t exponentially decreases with increasing distance from the shoreline—inconsistent with the field data, particularly at inland locations (e.g., W04). The agreement between calculated α_t and α_t simulated with the final model at all locations, and most notably at W04, supports the conceptualization that propagation of the tidal signal to shallow depth at inland areas

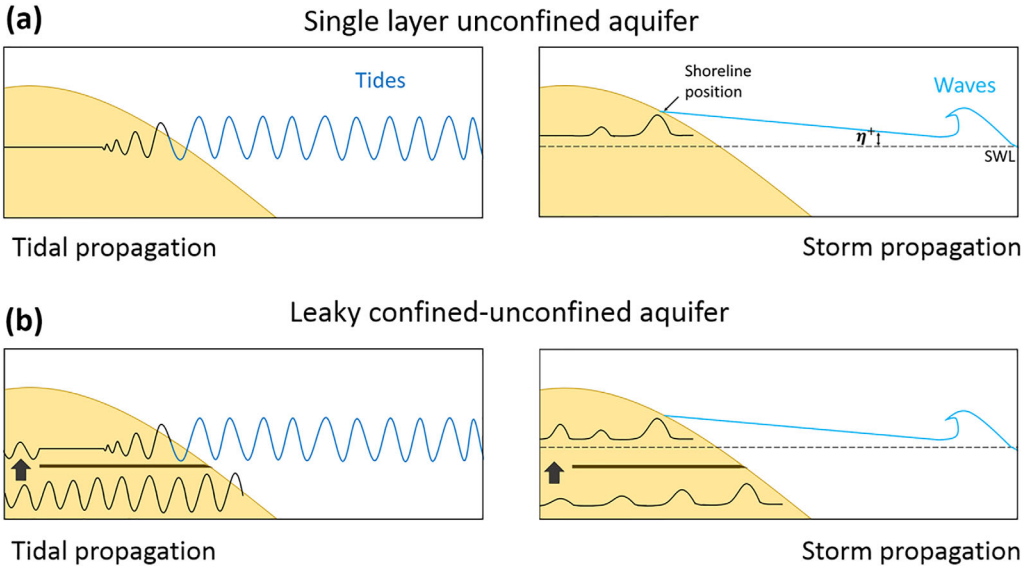

Figure 10. Conceptual diagrams illustrating the propagation of the tidal signal and offshore storm pulse signal through (a) a homogeneous unconfined aquifer system, versus (b) a leaky confined-unconfined aquifer connected to the ocean offshore and with localized leakage landward of the shoreline. Tidal signal propagation is shown separately on the left, and storm pulse signal propagation is shown separately on the right where breaking waves cause an upward tilt of the mean surface water level above the still water level (SWL) which is termed wave setup ($\eta+$).

is through leakage from an underlying confined aquifer. The final model was also able to reasonably simulate the location of the saltwater wedge inferred from geophysical surveys conducted by Hennigar (1976) (see Figure S2 in the supporting information for this comparison).

Simulations conducted with various aquitard configurations (i.e., cases 4–9) showed that a sloping aquitard near the shoreline was required to effectively dampen the water table fluctuations between W01 and W02 with negligible fluctuations at W03, while simultaneously matching the magnitude of the tide-induced fluctuations observed further inland at W04 (Area 1). The amplitude of the fluctuations in both the nearshore (W01) and inland (W04) areas could not be simulated with a flat aquitard (i.e., $\beta_{aqt} = 0$; cases 6–7). Sensitivity analyses also illustrated the effects of the tidal signal being damped vertically as it propagated upward

Table 2
Simulated and Calculated (From Field Fata) Amplitude Attenuation Factors (α_t) for Select Sensitivity Simulation Cases

Case	Parameter varied	W01 (error)	W02 (error)	W03 (error)	W04 (error)
	Calculated α_t from field data	0.11	0.017	0.005	0.091
1	Final model (Figure 2)	0.099 (−0.011)	0.025 (0.008)	1.3E-04 (–)	0.083 (−0.008)
2	Homogeneous unconfined aquifer ($d = 300$ m)	0.19 (0.08)	0.11 (−0.093)	0.021 (0.016)	0.013 (−0.078)
3	$\beta_{beach} = 0.05$, aquitard extends 10 m offshore	0.10 (−0.01)	0.027 (0.01)	1.1E-04 (–)	0.079 (−0.012)
Influence of Aquitard Configuration					
4	$\beta_{aqt} = 0.11$; $d_{W04} = 1.6$ m, $d_{W01} = 16.6$ m.	0.13 (0.02)	0.043 (0.026)	1.4E-04 (–)	0.078 (−0.013)
5	$\beta_{aqt} = 0.066$; $d_{W04} = 4.6$ m, $d_{W01} = 10.6$ m.	0.099 (−0.011)	0.026 (0.009)	1.6E-04 (–)	0.064 (−0.027)
6	$\beta_{aqt} = 0$; $d = 1.6$ m	0.0045 (−0.11)	2.6E-04 (−0.017)	1.1E-04 (–)	0.092 (−0.001)
7	$\beta_{aqt} = 0$; $d = 13.6$ m	0.10 (−0.01)	0.030 (0.013)	0.0013 (-0.0037)	0.035 (−0.056)
8	Aquitard thickness = 2 m	0.099 (−0.011)	0.025 (0.008)	6.1E-05 (–)	0.079 (−0.012)
9	$K_{aqt} = 0.005$ m/d	0.099 (−0.011)	0.025 (0.008)	4.8E-04 (–)	0.082 (−0.009)
Influence of Discontinuity Width and Location					
10	No discontinuity	0.098 (−0.012)	0.025 (0.008)	4.4E-04 (–)	0.001 (−0.09)
11	Shifted 10 m seaward	0.098 (−0.012)	0.025 (0.008)	1.3E-04 (–)	0.041 (−0.05)
12	Shifted 10 m landward	0.098 (−0.012)	0.025 (0.008)	8.9E-05 (–)	0.034 (−0.057)
13	5 m wide	0.099 (−0.011)	0.025 (0.008)	1.2E-04(–)	0.079 (−0.012)
14	20 m wide	0.099 (−0.011)	0.025 (0.008)	1.2E-04(–)	0.077 (−0.014)

Note. The error between the simulated and calculated α_t are provided in brackets.

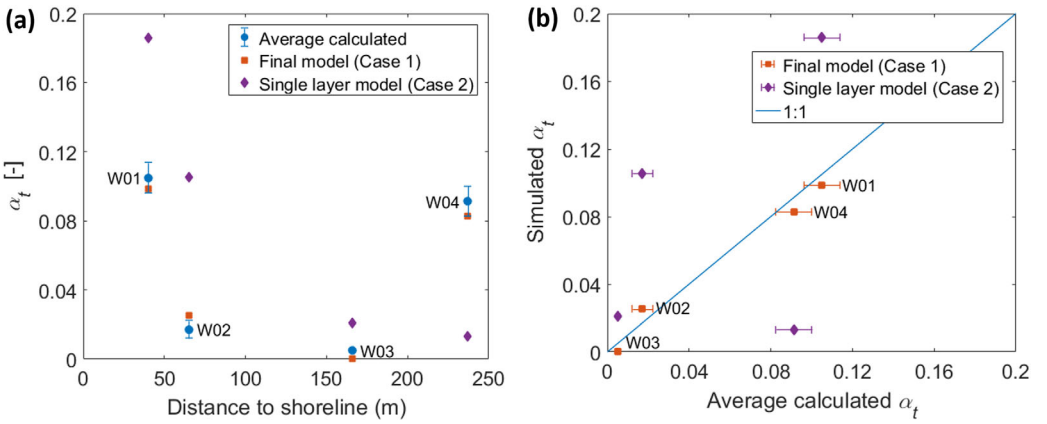

Figure 11. (a) Calculated amplitude attenuation factors α_t at monitoring wells versus distance to the shoreline, compared to simulated α_t for the final leaky confined-unconfined aquifer model (case 1, Table 2, Figure 2) and a single layer homogeneous unconfined aquifer model (case 2, Table 2). (b) Amplitude attenuation factors α_t at monitoring wells simulated for the final leaky confined-unconfined aquifer and homogeneous unconfined aquifer model setups, versus average calculated α_t. Error bars indicate the ranges of α_t calculated from the field data.

through the discontinuity into the unconfined aquifer. For instance, the amplitude of the water table fluctuation at W04 was considerably smaller when the inland unconfined aquifer depth (i.e., d_{W04}, Figure 2) increased from 1.6 m (final model, $\alpha_T = 0.0083$) to 13.6 m (case 7, $\alpha_T = 0.035$). For the conditions simulated, the aquitard thickness (1 m in final model and 2 m in case 8) and conductivity ($K_{aqt;} = 0.001$ m/d in final model and 0.005 m/d in case 9) had negligible effect on tidal signal propagation. Best match between the calculated and simulated water table fluctuations inland (i.e., at W04) was achieved with a 10 m wide discontinuity in the aquitard. Simulations (cases 10–14) were conducted to determine the influence of the location and width of this discontinuity. The water table fluctuations were greatest at W04 when the leak was located directly below the monitoring well (i.e., compare final model with cases 11–12 with the location of the leak shifted seaward and landward, respectively), and of medium width (10 m). If the width of the leakage was smaller (case 13, discontinuity = 5 m wide) the propagation of the tidal signal upward was too weak; however, if the leak was wider the tidal pressure signal from the confined aquifer rapidly dispersed and weakened as it propagated upward (case 14, discontinuity = 20 m wide). Finally, the configuration of the aquifer-ocean interface also influences the propagation of the tidal signal. Tidal propagation through the unconfined aquifer was slightly less attenuated when a smaller beach slope was simulated (i.e., case 3, $\beta_{beach} = 0.05$) compared to the final model, but more attenuated at the inland location W04. This is because the beach slope changes the wave setup profile (Nielsen, 2009) and therefore, based on our data analysis, the aquitard layer would extend 10 m seaward of the shoreline if $\beta_{beach} = 0.05$ (cf. final model with $\beta_{beach} = 0.10$ and aquitard layer extending 5 m seaward of the shoreline). Increasing the offshore extent of the aquitard ultimately decreases the simulated water table fluctuations at W04. Additional simulation results for varying boundary conditions (e.g., distributed recharge rate) and aquifer parameters (e.g., S_y) are provided in the supporting information Text S2 and Table S2.

4. Conclusions

Analysis of both tide- and storm-induced water table fluctuations was used for the first time to provide insight into the structural configuration of a coastal aquifer system. Signal propagation observed across the study site was discontinuous with isolated areas (up to ~400 m inland from the shoreline) found to experience large water table fluctuations with only a short time lag in the fluctuations relative to the driving oceanic forcing signals. Data analyses indicate water table fluctuations at isolated inland areas are likely due to upward leakage of the oceanic pressure signals from a lower confined aquifer, through which signal propagation is rapid, into a shallow unconfined aquifer. An aquitard layer with isolated discontinuities may have formed across the study area from the burial of organic material associated with relic surface water features. Comparison of the tide- and offshore storm-induced propagation rates enabled the connectivity between

the confined aquifer and the ocean to be inferred. The greater attenuation of the storm pulse signal at the isolated inland areas, despite similar phase lags to wells near the shoreline, suggests that the confined aquifer is exposed to a weaker driving storm pulse signal at the seaward boundary compared to the unconfined aquifer. This may occur if the confined aquifer is connected to the ocean seaward of the shoreline since the storm-induced wave setup profile would result in a weaker driving signal offshore relative to the shoreline setup signal which acts on the unconfined aquifer. Our hydrogeological conceptualization inferred from the data analyses was supported through numerical simulations of tidal signal propagation though a leaky confined-unconfined aquifer system. Further, sensitivity simulations illustrate the impact of the aquitard configuration (depth, slope, width of the leakage feature, etc.) on the propagation of tides through these multilayer coastal aquifer systems. This study shows that practical use of a combined approach of analyzing signal propagation of both tidal and storm pulse signals can provide important insight into the structure of a heterogeneous coastal aquifer system. Methods used in this study may be applied for low-cost large-scale hydrogeological investigations in coastal areas, and may be particularly useful for remote sites where access is challenging. Improved characterization of coastal aquifers is needed to guide effective water resource management decisions for the protection of coastal aquifers worldwide.

Acknowledgments
This study was financially supported by Parks Canada. The authors would like to thank Darren White, Jeremy Archer, and Alaina Lesley from the Environmental Sciences Group (ESG) for their assistance with the field logistics and data collection. Field data, sensitivity numerical modeling results, and details on numerical model development are provided in the supporting information. In addition, all field data and final model input files used to produce the results of this paper are available from the data set listed in the references (Trglavcnik et al., 2017).

References

Alcolea, A., Castro, E., Barbieri, M., Carrera, J., & Bea, S. (2007). Inverse modeling of coastal aquifers using tidal response and hydraulic tests. *Ground Water*, *45*, 711–722. https://doi.org/10.1111/j.1745-6584.2007.00356.x

Asadi-Aghbolaghi, M., Chuang, M.-H., & Yeh, H.-D. (2014). Groundwater response to tidal fluctuation in an inhomogeneous coastal aquifer-aquitard system. *Water Resources Management*, *28*, 3591–3617. https://doi.org/10.1007/s11269-014-0689-9

Carr, P. A., & Van Der Kamp, G. S. (1969). Determining aquifer characteristics by the tidal method. *Water Resources Research*, *5*, 1023–1031. https://doi.org/10.1029/WR005i005p01023

Cartwright, N. (2004). *Groundwater dynamics and the salinity structure in sandy beaches* (PhD thesis). Brisbane, QLD: University of Queensland.

Cartwright, N., & Gibbes, B. (2011). *Oceanic pulse forcing of a beach groundwater system*. Paper presented at 20th Australasian Coastal and Ocean Engineering Conference 2011, COASTS 2011 and the 13th Australasian Port and Harbour Conference 2011, PORTS 2011, Curan Associates Inc., Perth, West Australia.

Cartwright, N., Nielsen, P., & Li, L. (2004). Experimental observations of watertable waves in an unconfined aquifer with a sloping boundary. *Advanced Water Resources*, *27*, 991–1004. https://doi.org/10.1016/j.advwatres.2004.08.006

Chang, Y. C., Jeng, D. S., & Yeh, H. D. (2010). Tidal propagation in an oceanic island with sloping beaches. *Hydrology and Earth System Sciences*, *14*, 1341–1351. https://doi.org/10.5194/hess-14-1341-2010

Chuang, M.-H., Huang, C. S., Li, G. H., & Yeh, H. D. (2010). Groundwater fluctuations in heterogeneous coastal leaky aquifer systems. *Hydrology and Earth System Sciences*, *14*, 1819–1826. https://doi.org/10.5194/hess-14-1819-2010

Chuang, M.-H., & Yeh, H.-D. (2008). Analytical solution for tidal propagation in a leaky aquifer extending finite distance under the sea. *Journal of Hydraulic Engineering*, *134*, 447–454. https://doi.org/10.1061/(ASCE)0733-9429(2008)134:4(447)

Crosbie, R. S., Binning, P., & Kalma, J. D. (2005). A time series approach to inferring groundwater recharge using the water table fluctuation method. *Water Resources Research*, *41*, W01008. https://doi.org/10.1029/2004WR003077

Danard, M., Munro, A., & Murty, T. (2003). Storm surge hazard in Canada. *Natural Hazards*, *28*, 407–434. https://doi.org/10.1023/A:1022990310410

Dean, R. G., & Dalrymple, R. A. (1984). *Water wave mechanics for engineers and scientists*. Englewood Cliffs, NJ: Prentice-Hall.

Environmental Sciences Group (ESG) (2015). *2015 supplementary phase III environmental site assessment and groundwater dynamics program. Sable Island National Park Reserve Sable Island, Nova Scotia*. Kingston, ON: Royal Military College of Canada.

Erskine, A. D. (1991). Effect of tidal fluctuation on a coastal aquifer in the UK. *Ground Water*, *29*, 556–562. https://doi.org/10.1111/j.1745-6584.1991.tb00547.x

Ferris, J. G. (1951). Cyclic fluctuations of water level as a basis for determining aquifer transmissibility. *International Association of Scientific Hydrology*, 148–155. https://doi.org/10.3133/70133368

Gelhar, L. W., Welty, C., & Rehfeldt, K. R. (1992). A critical review of data on field-scale dispersion in aquifers. *Water Resources Research*, *28*, 1955–1974. https://doi.org/10.1029/92WR00607

Geng, X., Boufadel, M. C., Xia, Y., Li, H., Zhao, L., Jackson, N. L., & Miller, R. S. (2014). Numerical study of wave effects on groundwater flow and solute transport in a laboratory beach. *Journal of Contaminant Hydrology*, *165*, 37–52. https://doi.org/10.1016/j.jconhyd.2014.07.001

Gourlay, M. R. (1992). Wave set-up, wave run-up, and beach water table: Interaction between surf zone hydraulics and groundwater hydraulics. *Coastal Engineering*, *17*, 93–144. https://doi.org/10.1016/0378-3839(92)90015-M

Guo, H., Jiao, J. J., & Li, H. (2010). Groundwater response to tidal fluctuation in a two-zone aquifer. *Journal of Hydrology*, *381*, 364–371. https://doi.org/10.1016/j.jhydrol.2009.12.009

Guo, Q., Li, H., Boufadel, M. C., Xia, Y., & Li, G. (2007). Tide-induced groundwater head fluctuation in coastal multi-layered aquifer systems with a submarine outlet-capping. *Advanced Water Resources*, *30*, 1746–1755. https://doi.org/10.1016/j.adwatres.2007.01.003

Hanslow, D., & Nielsen, P. (1993). Shoreline set-up on natural beaches. *Journal of Coastal Research*, *15*, 1–10.

Hennigar, T. W. (1976). *Water resources and environmental geology of Sable Island, Nova Scotia* (Rep. 76-1). Nova Scotia, CA: Nova Scotia Department of Environment.

Hsieh, P. C., Hsu, H. T., Liao, C. B., & Chiueh, P. T. (2015). Groundwater response to tidal fluctuation and rainfall in a coastal aquifer. *Journal of Hydrology*, *521*, 132–140. https://doi.org/10.1016/j.jhydrol.2014.11.069

Huang, C.-S., Yeh, H.-D., & Chang, C.-H. (2012). A general analytical solution for groundwater fluctuations due to dual tide in long but narrow islands. *Water Resources Research*, *48*, W05508. https://doi.org/10.1029/2011WR011211

Jacob, C. E. (1950). Flow of groundwater. In H. Rouse (Ed.), *Engineering hydraulics* (pp. 321–386). Hoboken, NY: John Wiley & Sons.

Jeng, D. S., Li, L., & Barry, D. A. (2002). Analytical solution for tidal propagation in a coupled semi-confined/phreatic coastal aquifer. *Advanced Water Resources*, *25*, 577–584. https://doi.org/10.1016/S0309-1708(02)00016-7

Jeng, D. S., Seymour, B. R., Barry, D. A., Li, L., & Parlange, J. Y. (2005). New approximation for free surface flow of groundwater: Capillarity correction. *Advanced Water Resources*, *28*, 1032–1039. https://doi.org/10.1016/j.advwatres.2004.05.012

Jha, M. K., Namgial, D., Kamii, Y., & Peiffer, S. (2008). Hydraulic parameters of coastal aquifer systems by direct methods and an extended tide-aquifer interaction technique. *Water Resources Management*, *22*, 1899–1923. https://doi.org/10.1007/s11269-008-9259-3

Jiao, J. J., & Tang, Z. (1999). An analytical solution of groundwater response to tidal fluctuation in a leaky confined aquifer. *Water Resources Research*, *35*, 747–751. http://doi.org/10.1029/1998WR900075

Kim, J. H., Lee, J., Cheong, T. J., Kim, R. H., Koh, D. C., Ryu, J. S., & Chang, H. W. (2005). Use of time series analysis for the identification of tidal effect on groundwater in the coastal area of Kimje, Korea. *Journal of Hydrology*, *300*, 188–198. http://doi.org/10.1016/j.jhydrol.2004.06.004

Kong, J., Xin, P., Hua, G. F., Luo, Z. Y., Shen, C. J., Chen, D., & Li, L. (2015). Effects of vadose zone on groundwater table fluctuations in unconfined aquifers. *Journal of Hydrology*, *528*, 397–407. http://doi.org/10.1016/j.jhydrol.2015.06.045

Langevin, C. D., Thorne, D. T., Jr., Dausman, A. M., Sukop, M. C., & Guo, W. (2008). *SEAWAT version 4: A computer program for simulation of multi-species solute and heat transport* (U.S. Geol. Surv. Tech. Methods 6-A22, 39 p.). Reston, VA: U.S. Geological Survey.

Li, L., & Barry, D. A. (2000). Wave-induced beach groundwater flow. *Advances in Water Resources*, *23*(4), 325–337. https://doi.org/10.1016/S0309-1708(99)00032-9

Li, G., & Chen, C. (1991). Determining the length of confined aquifer roof extending under the sea by the tidal method. *Journal of Hydrology*, *123*, 97–104. https://doi.org/10.1016/0022-1694(91)90071-O

Li, H., & Jiao, J. J. (2001). Tide-induced groundwater fluctuation in a coastal leaky confined aquifer system extending under the sea. *Water Resources Research*, *37*, 1165–1171. https://doi.org/10.1029/2000WR900296

Li, L., Barry, D. A., & Jeng, D. S. (2001). Tidal fluctuations in a leaky confined aquifer: dynamic effects of an overlying phreatic aquifer. *Water Resources Research*, *37*, 1095–1098. https://doi.org/10.1029/2000WR900402

Li, L., Barry, D. A., Stagnitti, F., & Parlange, J. Y. (1999). Submarine groundwater discharge and associated chemical input to a coastal sea. *Water Resources Research*, *35*, 3253–3259. https://doi.org/10.1029/1999WR900189

Li, L., Barry, D. A., Stagnitti, F., & Parlange, J. Y. (2000a). Groundwater waves in a coastal aquifer: A new governing equation including vertical effects and capillarity. *Water Resources Research*, *36*, 411–420. https://doi.org/10.1029/1999WR900307

Li, L., Barry, D. A., Stagnitti, F., Parlange, J. Y., & Jeng, D. S. (2000b). Beach water table fluctuations due to spring-neap tides: Moving boundary effects. *Advanced Water Resources*, *23*, 817–824. https://doi.org/10.1016/S0309-1708(00)00017-8

Li, L., Cartwright, N., Nielsen, P., & Lockington, D. (2004). Response of coastal groundwater table to offshore storms. *China Ocean Engineering*, *18*, 423–431.

Li, L., Jeng, D. S., & Barry, D. A. (2002). Tidal fluctuations in a leaky confined aquifer: Localised effects of an overlying phreatic aquifer. *Journal of Hydrology*, *265*, 283–287. https://doi.org/10.1016/S0022-1694(02)00104-X

Longuet-Higgins, M. S. (1983). Wave set-up, percolation and undertow in the surf zone. *Proceedings of the Royal Society of London A*, *390*, 283–291.

Merritt, M. L. (2004). *Estimating hydraulic properties of the Floridan aquifer system by analysis of earth-tide, ocean-tide, and barometric effects, Collier and Hendry counties, Florida* (U.S. Geol. Surv. Water-Resour. Invest. Rep. 03–4267) Tallahassee, FL: U.S. Geological Survey.

Moore, W. S. (2010). The effect of submarine groundwater discharge on the ocean. *Annual Review of Marine Science*, *2*, 59–88. https://doi.org/10.1146/annurev-marine-120308-081019

Mulligan, A. E., Langevin, C., & Post, V. E. (2011). Tidal boundary conditions in Seawat. *Ground Water*, *49*, 866–879. https://doi.org/10.1111/j.1745-6584.2010.00788.x

Nielsen, P. (1990). Tidal dynamics of the water table in beaches. *Water Resources Research*, *26*, 2127–2134. https://doi.org/10.1029/WR026i009p02127

Nielsen, P. (2009). *Coastal and estuarine processes* (342 p.). Singapore,.

Nielsen, P., Aseervatham, R., Fenton, J. D., & Perrochet, P. (1997). Groundwater waves in aquifers of intermediate depths. *Advances Water Resources*, *20*, 37–43. https://doi.org/10.1016/S0309-1708(96)00015-2

Post, V. E. A. (2011). A new package for simulating periodic boundary conditions in MODFLOW and SEAWAT. *Computers and Geosciences*, *37*, 1843–1849. https://doi.org/10.1016/j.cageo.2011.01.012

Raubenheimer, B., Guza, R. T., & Elgar, S. (1999). Tidal water table fluctuations in a sandy ocean beach. *Water Resources Research*, *35*, 2313–2320. https://doi.org/10.1029/1999WR900105

Robinson, C., Gibbes, B., Carey, H., & Li, L. (2007). Salt-freshwater dynamics in a subterranean estuary over a spring-neap tidal cycle. *Journal of Geophysical Research: Oceans*, *112*, C09007. https://doi.org/10.1029/2006JC003888

Röper, T., Greskowiak, J., & Massmann, G. (2015). Instabilities of submarine groundwater discharge under tidal forcing. *Limnology and Oceanography Methods*, *60*, 22–28. https://doi.org/10.1002/lno.10005.

Rotzoll, K., & El-Kadi, A. I. (2008). Estimating hydraulic properties of coastal aquifers using wave setup. *Journal of Hydrology*, *353*, 201–213. https://doi.org/10.1016/j.jhydrol.2008.02.005

Rotzoll, K., El-Kadi, A. I., & Gingerich, S. B. (2008). Analysis of an unconfined aquifer subject to asynchronous dual-tide propagation. *Ground Water*, *46*, 239–250. https://doi.org/10.1111/j.1745-6584.2007.00412.x

Shih, D. C. F., Lin, G. F., Jia, Y. P., Chen, Y. G., & Wu, Y. M. (2008). Spectral decomposition of periodic ground water fluctuation in a coastal aquifer. *Hydrological Processes*, *22*, 1755–1765. https://doi.org/10.1002/hyp.6781

Slooten, L. J., Carrera, J., Castro, E., & Fernandez-Garcia, D. (2010). A sensitivity analysis of tide-induced head fluctuations in coastal aquifers. *Journal of Hydrology*, *393*, 370–380. https://doi.org/10.1016/j.jhydrol.2010.08.032

Song, Z., Li, L., Kong, J., & Zhang, H. (2007). A new analytical solution of tidal water table fluctuations in a coastal unconfined aquifer. *Journal of Hydrology*, *340*, 256–260. https://doi.org/10.1016/j.jhydrol.2007.04.015

Sun, P., Li, H., Boufadel, M. C., Geng, X., & Chen, S. (2008). An analytical solution and case study of groundwater head response to dual tide in an island leaky confined aquifer. *Water Resources Research*, *44*, W12501. https://doi.org/10.1029/2008WR006893

Teo, H. T., Jeng, D. S., Seymour, B. R., Barry, D. A., & Li, L. (2003). A new analytical solution for water table fluctuations in coastal aquifers with sloping beaches, *Advanced Water Resources*, *26*, 1239–1247. https://doi.org/10.1016/j.advwatres.2003.08.004

Trefry, M. G., & Bekele, E. (2004). Structural characterization of an island aquifer via tidal methods. *Water Resources Research*, *40*, W01505. https://doi.org/10.1029/2003WR002003

Trglavcnik, V., Morrow, D., Weber, K. P., Li, L., & Robinson, C. E. (2017). *Supporting dataset: "Analysis of tide and offshore storm-induced water table fluctuations for structural characterization of a coastal island aquifer" [Dataset]*. Zenodo. https://doi.org/10.5281/zenodo.1009584

Turner, I. L., Coates, B. P., & Acworth, R. I. (1997). Tides, waves and the super-elevation of groundwater at the coast. *Journal of Coastal Research*, *13*, 46–60.

Van Der Kamp, G. (1972). Tidal fluctuations in a confined aquifer extending under the sea. *24th International Geological Congress* (Section 11. pp 101–106). Montreal: J E Gill.

Van Der Kamp, G., & Gale, J. E. (1983). Theory of earth tide and barometric effects in porous formations with compressible grains. *Water Resources Research*, *19*, 538–544. https://doi.org/10.1029/WR019i002p00538

Wang, Q., Zhan, H., & Tang, Z. (2013). Groundwater response to dual tidal fluctuations in a peninsula or an elongated island. *International Journal for Numerical and Analytical Methods in Geomechanics*, *37*, 2456–2470. https://doi.org/10.1002/nag.2144

Wu, S. Y., Yarnal, B., & Fisher, A. (2002). Vulnerability of coastal communities to sea-level rise: A case study of Cape May County, New Jersey, USA. *Climate Research*, *22*(3), 255–270.

Xia, Y., Li, H., Boufadel, M. C., Guo, Q., & Li, G. (2007). Tidal wave propagation in a coastal aquifer: Effects of leakages through its submarine outlet-capping and offshore roof. *Journal of Hydrology*, *337*, 249–257. https://doi.org/10.1016/j.jhydrol.2007.01.036